The length-scale distribution function of the distance between extremal points in passive scalar turbulence

By LIPO WANG AND NORBERT PETERS

Institut für Technische Verbrennung, RWTH-Aachen, Templergraben 64, Aachen, Germany

In order to extract small-scale statistical information from passive scalar fields obtained by direct numerical simulation (DNS) a new method of analysis is introduced. It consists of determining local minimum and maximum points of the fluctuating scalar field via gradient trajectories starting from every grid point in the directions of ascending and descending scalar gradients. The ensemble of grid cells from which the same pair of extremal points is reached determines a spatial region which is called a 'dissipation element'. This region may be highly convoluted but on average it has an elongated shape with, on average, a nearly constant diameter of a few Kolmogorov scales and a variable length that has the mean of a Taylor scale. We parameterize the geometry of these elements by the linear distance between their extremal points and their scalar structure by the absolute value of the scalar difference at these points.

The joint p.d.f. of these two parameters contains most of the information needed to reconstruct the statistics of the scalar field. It is decomposed into a marginal p.d.f. of the linear distance and a conditional p.d.f. of the scalar difference. It is found that the conditional mean of the scalar difference follows the 1/3 inertial-range Kolmogorov scaling over a large range of length-scales even for the relatively small Reynolds number of the present simulations. This surprising result is explained by the additional conditioning on minima and maxima points.

A stochastic evolution equation for the marginal p.d.f. of the linear distance is derived and solved numerically. The stochastic problem that we consider consists of a Poisson process for the cutting of linear elements and a reconnection process due to molecular diffusion. The resulting length-scale distribution compares well with those obtained from the DNS.

1. Introduction

There have been many attempts to define the geometrical elements that one intuitively believes to represent 'eddies' of different size in turbulent flows. Discussions go back to Townsend (1951) who suggested that turbulent motion is essentially a random distribution of vortex sheets and tubes. More recently, Wray & Hunt (1990) subdivided the three-dimensional vortical field obtained from direct numerical simulations (DNS) into four types of space-filling regions, classifying them tentatively by characteristic values of the second invariant of the velocity derivative tensor as well as by the pressure.

Basically, eddies are statistical entities and any statistical evaluation in terms of a distribution function, for example, requires a clear definition of the quantity to be sampled. When eddies are viewed as random geometrical elements, the subject of

geometrical statistics in turbulence must be addressed. Corrsin (1971) differentiates between points, lines, surfaces and volumes that may be of possible physical interest and asks the following questions: "(1) What types (of geometry) are 'naturally' identifiable in turbulent flows? (2) What roles do they play or what properties do they have? and (3) What stochastic games can we invent which share some of the difficulties of the turbulent case, but are more treatable?"

It is clear that in order to address these questions one first needs to construct a suitable method which can identify specific geometrical elements in the turbulent flow. Which method one should choose is by no means evident. Tsinober (2001) points to the generic ambiguity in defining the meaning of scales and argues that it depends on the chosen decomposition/representation such as Fourier, Wavelet, proper orthogonal (POD) and others. These methods typically only analyse the dependent variables and their derivatives in a turbulent field in order to extract statistical properties, but they are not focused on geometry as such. Even fractal or multifractal analysis, which clearly addresses aspects of geometry, reduces the information to scaling exponents or other properties of self-similar geometry, cf. Meneveau & Sreenivasan (1991) and Frisch (1995). Interestingly, in Tsinober (2001), there are three sections, each entitled "Geometrical statistics", within chapters 4, 6 and 7. Here statistics of gradients of velocity and scalars as well as local alignments are discussed, but no references to papers dealing with the statistics of finite-size structures are given. This lack of relevant work is probably due to the difficulty of clearly defining shapes and length scales in turbulence.

An attempt to overcome this problem was made by Miyauchi & Tanahashi (2001). They visualized contour surfaces of the second invariant of the velocity gradient tensor and thereby identified tube-like vortex filaments in homogeneous turbulent shear flows generated by DNS. Then they divided those filaments into segments between local minima of the second invariant. They derived p.d.f.s of segment length normalized by the Taylor microscale and concluded that the fine-scale structure is directly related to that scale. Another example for length-scale p.d.f.s is found in Jimenez & Wray (1998) for the radius of vortex filaments. In a log-linear plot these p.d.f.s display an exponential decay for large length scales, a property that we will rediscover for the length-scale distribution in this paper. Also, when the data of Miyauchi & Tanahashi (2001) are replotted on a log-linear scale, an exponential tail is found, the slope of which, however, depends on the Reynolds number.

The objective of the present paper is to set the basis for prediction methods of scalar fields that incorporate information from length scales below the integral scales. Of particular interest for us are the p.d.f. of the scalar ϕ and the conditional scalar dissipation rate $\langle \chi | \phi \rangle$ where the instantaneous dissipation rate is defined as $\chi = 2D(\nabla \phi')^2$, since these are required for the prediction of turbulence–chemistry interaction in non-premixed turbulent combustion, cf. Peters (2000). Previous attempts to model them on the basis of integral quantities such as the turbulent kinetic energy, its dissipation and the scalar mean and variance using presumed shapes must remain unsatisfactory, because they do not take small-scale information into account. The influence of heat release on the shape of the conditional scalar dissipation was investigated by Pantano, Sarkar & Williams (2003) using DNS.

In order to capture the small-scale structure of the fluctuating scalar field we will subdivide it into finite-size regions within which it varies monotonically. For illustration, part of a larger two-dimensional scalar field is sketched in figure 1, showing four maximum points which are grouped around one central minimum point. By analogy to geological topography this configuration may be identified as
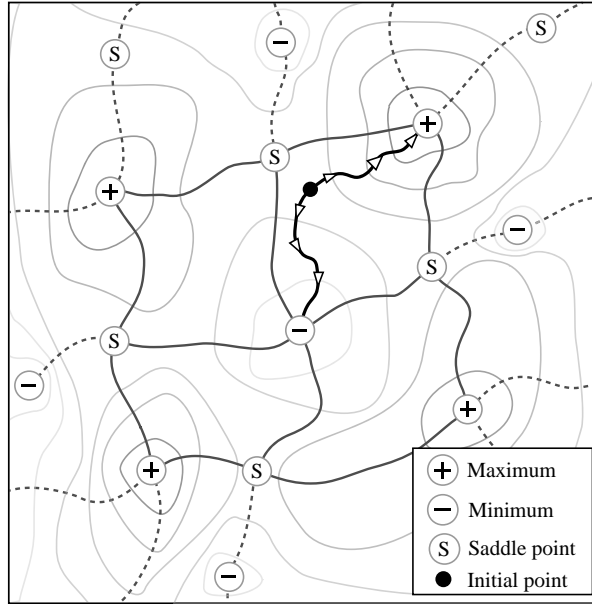
FIGURE 1. Schematic sketch of a two-dimensional scalar field including the trajectories from an initial point to the minimum and maximum points. The solid lines are geodetic lines bounding four repeating units corresponding to dissipation elements, while the dashed lines are geodetic beyond these units.

a crater surrounded by a closed ridge line having four local summits. There are four more minimum points at the periphery. Also shown are iso-scalar lines around these extremal points and geodetic lines that connect two maxima or minima and pass through a saddle point. It is evident that along the geodetic lines the scalar gradient in the normal directions vanishes. There are four repeating units bounded by geodetic lines shown in figure 1 in which the scalar field varies monotonically. These regions may be identified numerically by placing a uniform grid over the entire domain and by starting trajectories from every grid point in the directions of ascending and descending scalar gradients. We will assume that the scalar field, due to the smoothing effects of diffusion, satisfies the conditions for a Morse function. This is a sufficiently smooth function which can be presented in a pure quadratic form in the vicinity of extremal points. Then D'Acunto & Kurdyka (2004) have shown that any local extremal point can be joint by a gradient trajectory of finite length. The two trajectories shown in the upper right repeating unit in figure 1 will then inevitably reach the minimum and the maximum points of the unit. The trajectories will not be able to leave the unit, which is bounded by zero normal gradient lines (in two-dimensions) or zero normal surfaces (in three-dimensions). *The ensemble of grid cells from which the same pair of minimum and maximum points are reached define a spatial region which will be called a dissipation element.*

Gibson (1968) was the first to analyse in detail the properties of zero-gradient points and minimal gradient surfaces in passive scalar turbulence with a mean scalar gradient. He pointed out that in one dimension the number of minimum and maximum points should be equal, while in two-dimensions their sum should be equal to the number of saddle points, as it is evident from figure 1. However, saddle points may merge such that extremal points are connected to fewer saddle points

than shown in figure 1. Even in the case where all saddle points connecting one extremal point have merged into a single one, the trajectories would also merge and follow the geodetic line to reach the extremal point. In three dimensions the topology may be much more complicated, cf. Moffatt (2001), and no definite prediction about the number of saddle points – and saddle lines, which are also possible in three dimensions – can be made. We have searched for ideal shapes of single dissipation elements that would fill the three-dimensional space uniformly. We found that a cube would be one example where the two extremal points lie at opposite corners while the other six corners would be saddle points. Another ideal shape is an octahedron having the two extremal points at the vertices and four saddle points, connected by saddle lines, at the corners of the square base. In order to fill a three-dimensional space subdivided into cubes uniformly, the vertices of the octahedrons have to be placed at the centre of the cubes, while the bases lie at the surfaces separating two cubes. However, the reality in three-dimensional turbulence is far from such ideal shapes as we will see below.

Having defined finite-size space-filling regions within which the fluctuating scalar field varies monotonically a first task should be to derive a model for the scalar fluctuations within these regions (expecting them to be smaller than for the entire field). This will be called the local structure. A second task must be to parameterize the shape of the region and the change of the scalar within it in terms of suitable parameters. Since these parameters p_i vary randomly one obtains a joint p.d.f. $P(p_i)$ of those parameters. Finally, the joint p.d.f. must be modelled. With these two models one should be able to reconstruct statistical properties such as the scalar p.d.f. or the conditional scalar dissipation rate. For instance, when the local scalar dissipation rate χ_L is known as a function of the scalar and of n parameters $p_1, p_2, \ldots, p_n$ the conditional scalar dissipation rate can be reconstructed from

$$\langle \chi | \phi \rangle = \iint \ldots \int \chi_L(\phi, p_1, p_2, \ldots, p_n) P(p_1, p_2, \ldots, p_n) \, \mathrm{d}p_1 \, \mathrm{d}p_2 \ldots \mathrm{d}p_n. \quad (1.1)$$

The first task was undertaken in Peters & Trouillet (2002) where models for the local structure of the p.d.f. and the scalar dissipation rate were derived for segments between minimum and maximum points of a one-dimensional scalar profile . These models were then used to reconstruct the scalar p.d.f. and the conditional scalar dissipation rate obtained from DNS of a turbulent mixing layer by Rogers & Moser (1994), showing reasonable agreement when the joint p.d.f. of the relevant parameters was taken from the DNS. Therefore we focus in this paper on the second task. We will analyse the joint p.d.f. of two of the parameters that we believe to be the most important: the linear distance between the minimum and the maximum of a dissipation element and the absolute value of the scalar difference at these points. A third parameter identified in Peters & Trouillet is the algebraic mean of the maximum and the minimum value of the scalar, but since this parameter turns out to be statistically independent of the two others, we will not include it here.

The paper is organized as follows: In the next section we will present the instantaneous and average shapes of the elements and draw a physical picture of how they interact with the turbulent flow which we visualize as vortex tubes and strain sheets. In §3 we will present the joint p.d.f. and show that the conditional mean of the scalar difference follows the Kolmogorov scaling law for the structure function, namely the 1/3 power law. In §4 we will derive a stochastic evolution equation for the length-scale distribution function by analysing the transition of grid cells between different classes of elements due to cutting and reconnection processes. The length

Case	1	2	3
No. of grid cells	256^3	512^3	128^3
Viscosity ν	0.01	0.003	0.01
r.m.s. velocity	1.58	1.304	1.1334
Turbulent kinetic energy k	3.75	2.55	1.927
Dissipation ε	1.64	0.939	0.905
Mean scalar variance $\langle \phi'^2 \rangle$	0.0538	0.0294	0.0242
Mean scalar dissipation $\langle \chi \rangle$	0.04453	0.0255	0.0226
$S k / \varepsilon$	3.430	4.073	3.194
No. of elements	7801	75 302	6476
No. of extremal points	2384	20 413	2052
Kolmogorov scale η	0.0279	0.013	0.0324
Taylor scale λ	0.478	0.285	0.4614
Mean length l_m	1.037	0.492	0.946
Re_λ	75.5	123.9	52.3
$\Delta x / \eta$	0.850	0.944	1.515

TABLE 1. Resolution and calculated turbulence parameters for three DNS cases.

scale will be defined as the linear distance between the minimum and the maximum points of an element. We will compare this distribution with those extracted from the DNS. The paper ends with a short outlook and conclusion.

2. Shapes and spatial distribution of dissipation elements

We have performed four DNS within a cubic box of 2π side length for homogeneous incompressible turbulent shear flow with an imposed velocity gradient $S = \mathrm{d}\langle u_1 \rangle / \mathrm{d}x_2 = 1.5$. In addition, the field of a passive scalar with unity Prandtl number and an imposed scalar gradient of $\mathrm{d}\langle \phi \rangle / \mathrm{d}x_2 = 1/(2\pi)$ was calculated. The three cases listed in table 1 differ by the number of grid cells and the choice of the viscosity ν, which varies from $\nu = 0.003$ for case 2 to $\nu = 0.01$ for cases 1 and 3. The Reynolds number based on the Taylor scale ranged from $Re_\lambda = 52.3$ to $Re_\lambda = 123.9$ as shown in table 1. In all cases the ratio of the grid length to the Kolmogorov scale $\Delta x / \eta$ is less than the limiting value of 2.1 suggested by Pope (2000), but for a sufficiently accurate calculation of trajectories a resolution of $\Delta x / \eta < 1$ was found to be necessary.

A spectral collocation method was used to transform the incompressible Navier–Stokes equations for velocity and the equation for the passive scalar as well as the Poisson equation for the pressure into Fourier space. A third-order Runge–Kutta algorithm was used for time advancement. The continuity equation was satisfied by adding to right-hand side of each of the momentum equations a negative decay term proportional to the respective velocity component and to the divergence of the velocity field. The code is an incompressible version of the spectral code by Sarkar (1995). From the Fourier coefficients not only the values of the passive scalar but also its derivatives in the three spatial directions can be calculated. In order to identify minima and maxima points trajectories in the directions of ascending and descending gradients were calculated starting from every grid point in the box. For this purpose the gradient fields were linearly interpolated during the marching process.

The scalar fields to be analysed were obtained in the three cases listed in table 1 at a time larger than 25 eddy turnover times when $S k / \varepsilon$, after an overshoot, tends to the theoretical plateau value of 3.3, around which it oscillated strongly, however. The theoretical plateau value follows from a balance of production and dissipation
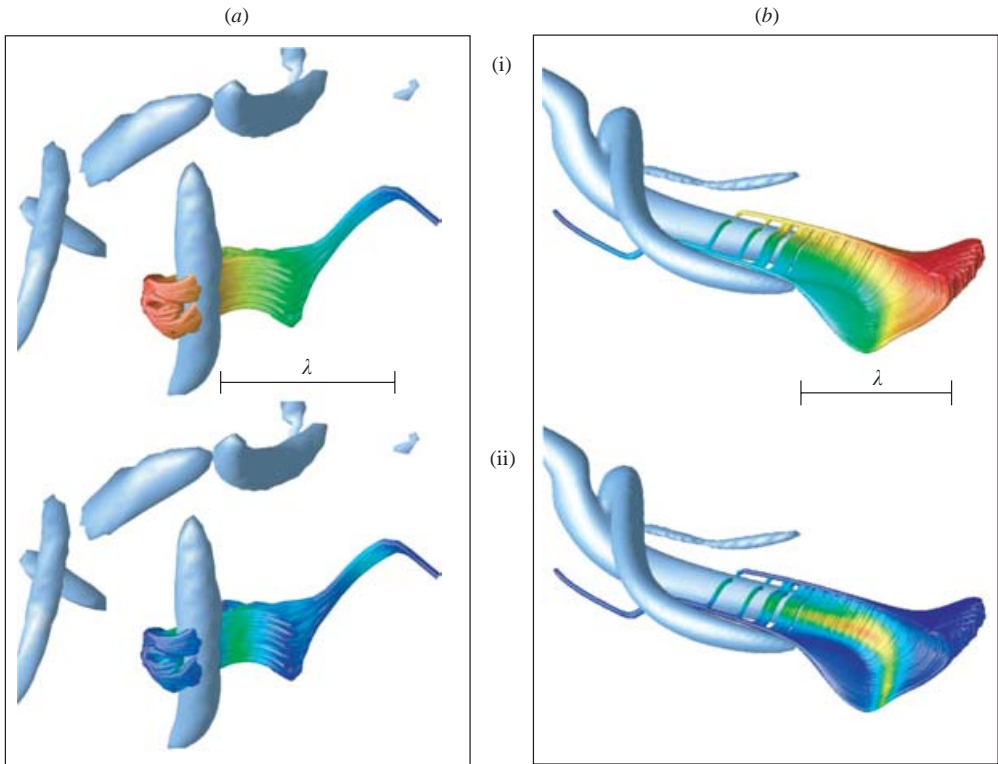
FIGURE 2. The interaction of a dissipation element with a vortex filament visualized from the DNS data of (a) case 3 and (b) case 1. (i) Trajectories are colour coded by the local value of the scalar; (ii) trajectories are colour coded by the local value of the scalar dissipation rate.

in the equation for the turbulent kinetic energy. In order to collect enough data for the statistics several consecutive scalar fields needed to be analysed by the gradient trajectory method. While data from only one field were used in case 2, 10 fields were needed in case 1 and 20 fields in case 3 covering a time span of up to three eddy turnover times. During that time span the turbulent kinetic energy did not change more than 10%.

Typical shapes of individual dissipation elements for the passive scalar field from cases 3 and 1 are shown in figures 2(a) and 2(b) together with vortex filaments. The shapes of the dissipation elements were obtained by plotting the trajectories between the minimum point and the maximum point of the fluctuating scalar. Their colour coding characterizes the value of the scalar (figures 2(a)(i) and 2(b)(i)) or the local scalar dissipation rate (figures 2(a)(ii) and 2(b)(ii)). The shapes of vortex filaments were obtained by visualizing contour surfaces of the second invariant of the velocity gradient tensor $Q = \omega^2 - s_{ij}s_{ij}$ where ω^2 is the enstrophy and s_{ij} is the strain tensor.

The dissipation element in figure 2(a)(i) is partly wrapped around such a vortex filament. The axis of this tube is nearly perpendicular to the overall scalar gradient, which is in the direction of a straight line between the scalar minimum (blue) on the right-hand side and the maximum (red) on the left-hand side. Such an orientation is in agreement with the picture drawn by Ashurst et al. (1987) of the local alignment of vorticity and scalar gradients. They found that among the three perpendicular strain directions there exists a high probability of alignment between scalar gradients

and the most compressive rate of strain, while vorticity preferentially aligns with the intermediate rate of strain.

In figure 2(a)(i) one observes a strong turning of the trajectories in the green region. This region probably corresponds to the vicinity of a vertical saddle line. On a saddle line itself the gradients in all three directions vanish and therefore the scalar dissipation rate is zero. To test this hypothesis we have colour coded the trajectories in figure 2(a)(ii) by the value of the local scalar dissipation rate, normalized between zero (blue) and its maximum value (red). In the vicinity of the scalar minimum and maximum points, the scalar dissipation rate is blue and therefore small, as expected. It increases in the region where the dissipation element interacts with the vortex filament, but decreases to very low values again in the region which we have interpreted to be close to a saddle line. There is another, but small, increase of the scalar dissipation rate on the elongated part on the right-hand side.

In many cases where dissipation elements closely interact with vortex filaments we find them to be perpendicular to each other. A counterexample is shown in figure 2(b)(i). This dissipation element is essentially aligned with two vortex filaments which are probably counter-rotating. The element is partly wrapped around the broader filament where it has a sheet-like shape. This sheet is bent upwards by the influence of the second thinner vortex filament. The main body of the element is towards the right-hand side where it becomes more volumetric. It becomes very thin towards the left-hand side where all trajectories eventually merge into a single line. This means that saddle points have merged in this region, probably because they have been squeezed together by the interacting vortex filaments. The merging of saddle points has been discussed in the introduction in the context of the two-dimensional illustration. Finally, in figure 2(b)(ii) the trajectories have been colour coded with the local scalar dissipation rate. Higher values of this quantity are again found in regions where the element is wrapped around the broader vortex filament. At the sharp upper and lower edges on the left-hand side of the element the scalar dissipation rate is again very low, which leads to the hypothesis that these edges correspond to saddle lines. The corner points on the right-hand side may be saddle points.

The visualization of two typical dissipation elements leads to the conclusion that they are more convoluted and irregular in shape than vortex filaments, but that they also are elongated structures. They are often flat near one extremal point with a sharp edge at the other. A major difference with vortex filaments is that they are space-filling by construction. Therefore adjacent elements, which often share one common extremal point, must be strongly intertwined which is difficult to visualize, at least if one wants to include vortex filaments as well.

Next we show how the elements are distributed within the cubic box. Blue minimum and red maximum points are shown for case 1 at a fixed time in figure 3. There is an approximately equal number of minimum and maximum points, the largest deviation from this equality being 1% for the higher Reynolds number case 2. For each dissipation element the minimum and maximum points have been connected by a straight yellow line. Also shown are isosurface contours of the negative value of the second invariant of the velocity derivative tensor Q which essentially represents the magnitude of the local strain rate. Differently from the previous picture these contours display a sheet-like and not a tube-like behaviour. The distribution of extremal points is quite irregular, but at certain locations strings of minimum or maximum points are observed. This is most evident for the string of red point in the central part of the figure. This string seems to be embedded in a surface of large strain rates. This may be a manifestation of the process of secondary splitting of extremal points by
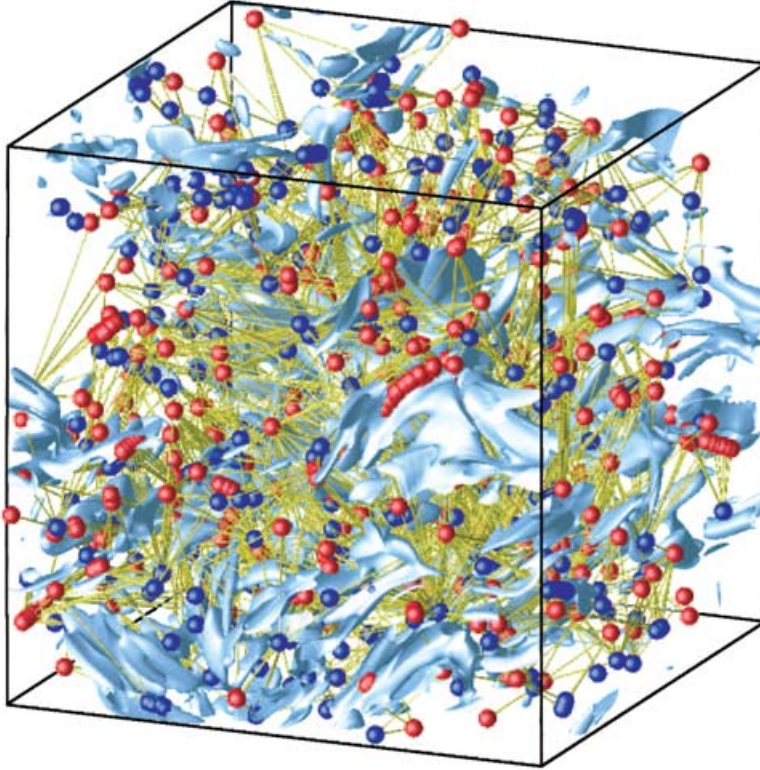
FIGURE 3. Distribution of extremal points and high-strain regions in the box. Red points are maxima, blue points are minima. They are connected by yellow straight lines for each dissipation element. Also shown are isosurface contours of the negative value of the second invariant of Q.

local strain, as analysed by Gibson (1968). The multiplication of extremal points by this process is probably responsible for the skewed shape of many of the dissipation elements.

We now analyse the average radius of dissipation elements by grouping them into classes characterized by their linear length. The volume of an element is given by multiplying the number of its grid cells by the grid cell volume. Dividing this by the linear length of the element provides a mean cross-sectional area. Equating this area to that of a cylindrical rod with diameter d provides a mean diameter of the element. Averaging the mean diameters of all elements in a class produces the surprising result shown in figure 4 that the average diameter varies little with linear length, and even has the tendency to decrease. Here, both the diameter and the linear length were normalized by the Kolmogorov scale η.

The average shape of all elements was obtained by subdividing the straight line between the minimum and maximum points of an element into several segments. All grid cells falling into the region between end planes normal to the straight line determine a partial volume of the dissipation element. The centre of gravity of those grid cells in the segment determines its distance from the straight line. It is normalized by the element length to determine the average span. Also, by equating the partial volume to that of a cylindrical rod with length equal to the segment length, a mean segment diameter was calculated. Normalizing it by the element length and averaging
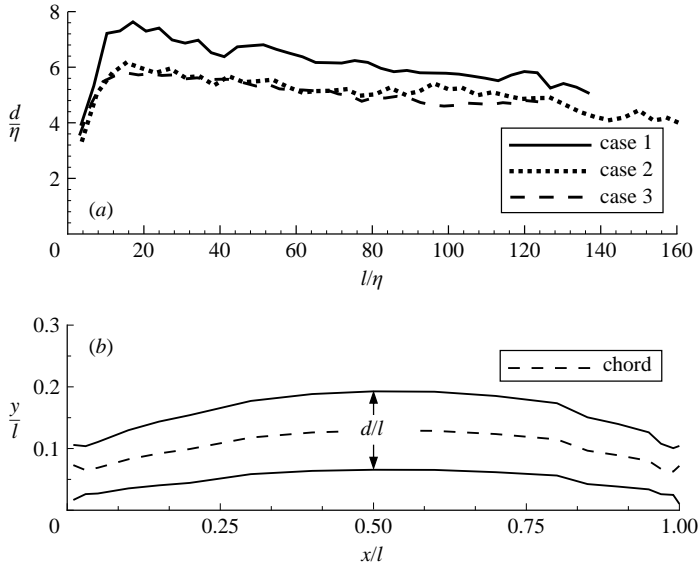
FIGURE 4. (a) Variation of the normalized diameter d/η with the normalized linear length l/η for the three DNS cases. (b) Average shape of elements of case 1.

over all classes provides the average diameter along the chord. This average shape of all elements from case 1, for example, is shown in figure 4(b). Here x denotes the coordinate along the straight line and y a coordinate normal to it.

3. The joint p.d.f. of the linear distance and the absolute value of the scalar difference

Among the many parameters that would potentially describe the statistical properties of the dissipation elements, we have chosen the linear distance $l = |\boldsymbol{x}_{max} - \boldsymbol{x}_{min}|$ between the minimum and maximum points and the absolute value of the fluctuating scalar difference $\Delta\phi' = |\phi'(\boldsymbol{x}_{max}) - \phi'(\boldsymbol{x}_{min})|$ at these points, where $\phi' = \phi(\boldsymbol{x}) - x_2 S_\phi$. Figure 5 shows, for case 1 as an example, the joint p.d.f. $P(\Delta\phi', l)$. We believe that this joint p.d.f. contains most of the information needed to reconstruct the statistics of the scalar field in terms of the integral and molecular quantities given in table 1. According to Bayes' theorem the joint p.d.f. can be written as the product of the conditional p.d.f. of the scalar difference $P_{\Delta\phi'}(\Delta\phi'|l)$ and the marginal p.d.f. $P_l(l)$:

$$P(\Delta\phi', l) = P_{\Delta\phi'}(\Delta\phi'|l)P_l(l), \tag{3.1}$$

where the marginal p.d.f. is defined by

$$P_l(l) = \int_0^\infty P(\Delta\phi', l)\,\mathrm{d}(\Delta\phi'). \tag{3.2}$$

Regarding the conditional p.d.f. $P_{\Delta\phi'}(\Delta\phi'|l)$, we first consider its conditional mean value

$$\langle\Delta\phi'|l\rangle = \int_0^\infty (\Delta\phi')P_{\Delta\phi'}(\Delta\phi'|l)\,\mathrm{d}(\Delta\phi'). \tag{3.3}$$

A linear-log plot of this mean compensated by $l^{1/3}$ versus the normalized linear length l is shown in figure 6 where the compensation is consistent with Kolmogorov's scaling.
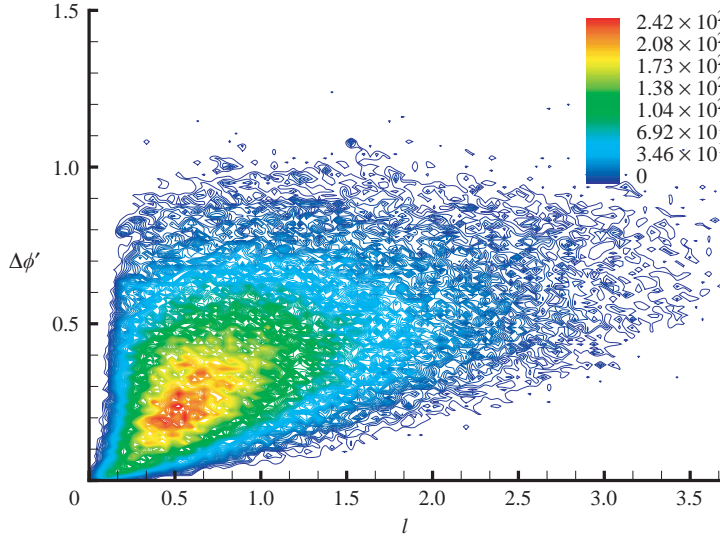
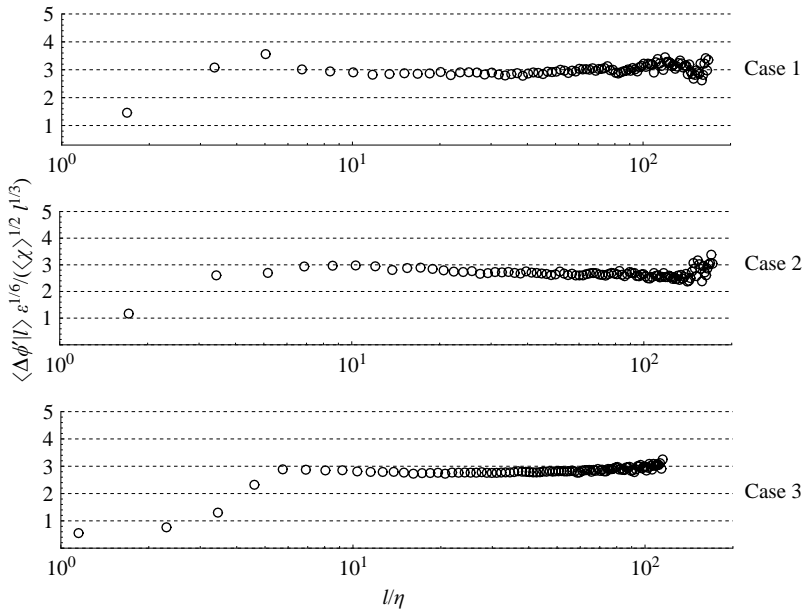FIGURE 5. The joint p.d.f. of the linear length and the scalar difference.

FIGURE 6. Compensated conditional mean scalar difference as function of the normalized linear length.

It is interesting to note that for all three cases the plot follows a horizontal line over the inertial range extending over more than one order of magnitude. The proportionality constant C_ϕ of the relation $\langle \Delta\phi'|l \rangle = C_\phi \langle \chi \rangle^{1/2} l^{1/3}/\varepsilon^{1/6}$ is around $C_\phi = 2.8$ for all three cases. It may be surprising that the inertial-range scaling starts at approximately 7η, which is much smaller than the values of 60η or higher quoted in the literature for
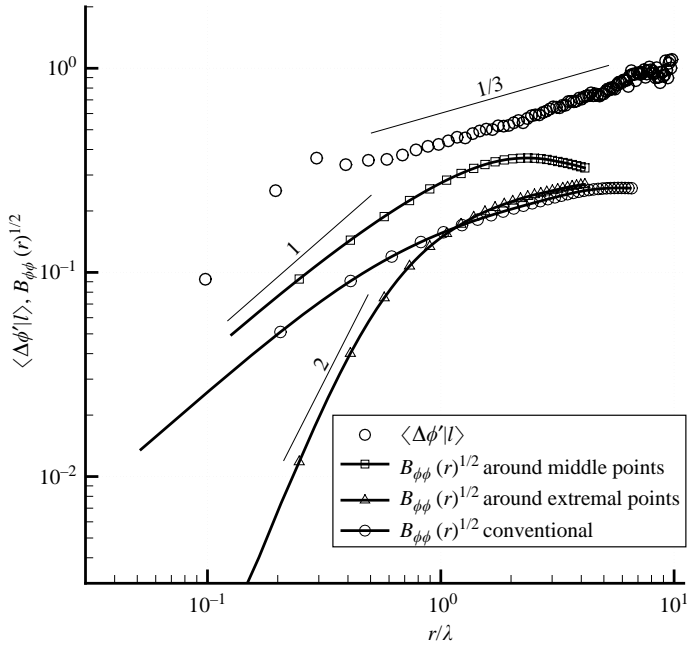
FIGURE 7. The conditional mean of the scalar difference $\langle \Delta \phi' | l \rangle$ compared with different versions of the structure function $B_{\phi\phi}^{1/2}$.

classical structure functions. There is a fundamental difference between the conditional mean scalar difference of dissipation elements and structure function scaling.

In order to understand this difference we have applied structure function analysis by conditioning it for case 1 to two distinctly different regions within our dissipation elements:

(*a*) to regions around the centre of dissipation elements where it starts at the mid-point in the direction of the straight line connecting the extremal points;

(*b*) to regions around local extremal points with structure functions in all directions. We compare these to the unconditional structure function $B_{\phi\phi}(r)$ and to the conditional mean value of the scalar difference. As shown in figure 7 the square root of the structure function for case (*a*) has a nearly unity exponent in the viscous-diffusive range – as it should according to Kolmogorov's scaling – but bends over within the inertial range. On the other hand, the square root of the structure function for case (*b*) has an exponent of 2 in the viscous diffusive range, and nearly coincides with the unconditional structure functions in the inertial range. The corresponding exponent 4 of the two-point correlation function can easily be explained by expanding it into a Taylor series around zero-gradient points. This also demonstrates that in the vicinity of extremal points the scalar field is more closely correlated. The observation that the unconditional structure function is embedded between the two conditional cases, following the second case more closely in the inertial range, suggests that classical structure function analysis for relatively small Reynolds numbers is considerably contaminated by more closely correlated regions around extremal points. The conditional mean value $\langle \Delta \phi' | l \rangle$ for dissipation elements may be viewed as representing the square root of the two structure functions starting from the mid-point of the elements along the straight line in both directions, but
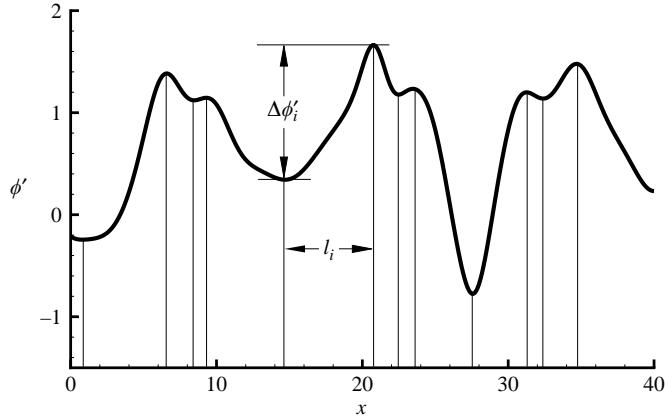
FIGURE 8. The scalar profile along the axis of linearly connected rod-like elements with linear length l_i and scalar difference $\Delta\phi'_i$.

ending precisely at the first extremal point. This additional conditioning means that they avoid the more highly correlated regions around the extremal points.

4. Theory

We have shown that, at least on average, the elements are elongated structures with diameter of a few Kolmogorov scales but a greatly varying length. We now are interested in the marginal probability density $P_l(l)$ of this length l. In order to model this p.d.f. we assume that elements are one-dimensional structures that are cut into pieces. Such cutting corresponds physically to the generation of extremal points. For this purpose we refer to Gibson (1968) who had also analysed the mechanism by which extremal points are generated. He notes that in the absence of diffusion, convective motion alone is unable to generate extremal points, because iso-scalar surfaces will just follow the fluid motion even if this leads to very large distortions of these surfaces (as one observes in high-Prandtl-number flows, for instance). Only a diffusion velocity of the same magnitude as the local convective velocity is able to generate extremal points. This analysis shows that extremal points are generated at scales of the Obukhov–Corrsin length $(D^3/\varepsilon)^{1/4}$ which in our case is equal to the Kolmogorov scale. According to this theory the generation of extremal points occurs randomly. As the local dynamics of this process is not fully understood we postulate a Poisson mechanism with constant frequency that cuts rod-like structures into shorter rods, assuming that their diameter remains unchanged. This will be called the cutting process. It will generate smaller elements by removing larger elements.

On the other hand, as dissipation elements are convected by the turbulent flow field, local minima and maxima may be swept into close proximity thus allowing diffusion to annihilate them. This corresponds in the one-dimensional picture of rod-like structures to the disappearance of very small elements and thereby the reconnection of adjacent larger elements. Imagine, for simplicity, a one-dimensional profile of the passive scalar ϕ' along the axes of such linearly connected rods, as shown in figure 8, where one can identify local minimum and maximum points as the end parts of the elements, each having a finite length l_i and a scalar difference $\Delta\phi'_i$. Since this profile is subjected to diffusion due to the nature of the diffusion equation, the local minima and maxima of very small elements move towards each other and disappear, thereby

reconnecting the adjacent larger elements. We will call this the reconnection process. It will generate larger elements by removing those that are reconnected. The very small elements between them have drifted, as they disappear in length-scale space towards zero. This will be called the drift process by diffusion. In addition there will be another drift process due to the relative velocity of two extremal points.

Let us first ignore the drift processes and consider only the cutting and the reconnection processes. Conceptually, we will divide the one-dimensional domain under consideration into grid cells of equal length using a uniform mesh. Then the length l of a dissipation element is proportional to the number of grid cells within it. We will consider the transition of the number n_l of grid cells within a class of elements of length l. This number is $n_l P_l(l) \mathrm{d}l$. The problem that we are considering is a birth-and-death process which is continuous in time. The time rate of change of the number of grid cells between different classes of elements follows a Boltzmann-type evolution equation, cf. Van Kampen (1992),

$$\frac{\partial}{\partial t}[n_x P_x(x, t)]\,\mathrm{d}x = \int W(x|y)n_y P_y(y, t)\,\mathrm{d}y\,\mathrm{d}x - \int W(y|x)n_x P_x(x, t)\,\mathrm{d}y\,\mathrm{d}x. \quad (4.1)$$

Here we have denoted by x the class under consideration, while y stands for the class from which transitions to x occur. Furthermore, $W(x|y)$ and $W(y|x)$ are the transition probability densities per unit time from y to x and from x to y, respectively. Usually $W(x|y)$ needs not to be equal to $W(y|x)$. The physics of the problem are contained in these transition probability densities.

The integrals in (4.1) represent the generation and removal of grid cells due to the cutting and reconnection processes mentioned above. Since both these processes generate and remove grid cells in class x there will be a total of four contributions to the rate of change of $n_x P_x(x, t)$, namely

   (i) the generation by the cutting process (gc);
  (ii) the removal by the cutting process (rc);
 (iii) the generation by the reconnection process (gr);
 (iv) the removal by the reconnection process (rr).

The disappearance of the very small elements due to merging by the drift process concerns the class $x = 0$ only and will determine the boundary condition as $P_x(0) = 0$.

After division by $\mathrm{d}x$ (4.1) then has four terms on the right-hand side

$$\frac{\partial}{\partial t}[n_x P_x] = \frac{\partial}{\partial t}[n_x P_x]_{\mathrm{gc}} + \frac{\partial}{\partial t}[n_x P_x]_{\mathrm{rc}} + \frac{\partial}{\partial t}[n_x P_x]_{\mathrm{gr}} + \frac{\partial}{\partial t}[n_x P_x]_{\mathrm{rr}}, \quad (4.2)$$

containing the transition probability densities $W_{\mathrm{gc}}(x|y)$, $W_{\mathrm{rc}}(y|x)$, $W_{\mathrm{gr}}(x|y)$ and $W_{\mathrm{rr}}(y|x)$, respectively. For the cutting process we first consider the generation (gc) of grid cells in the class of smaller elements of size x from those of a larger element of size y. The time rate of change due to this process is therefore

$$\frac{\partial}{\partial t}[n_x P_x]_{\mathrm{gc}} = \int_x^\infty W_{\mathrm{gc}}(x|y)n_y P_y(y, t)\,\mathrm{d}y. \quad (4.3)$$

Since elements of the fixed class x are obtained by cutting elements of a class y, where $y > x$, the integration is performed from x to ∞. The transition probability density per unit time $W_{\mathrm{gc}}(x|y)$ is proportional to a rate ω (number of effective cuttings per unit time) times the probability density $P_{y \to x}(x, y)$ that such cutting generates elements of class x. Therefore we obtain

$$W_{\mathrm{gc}}(x|y) = \omega(y)\,P_{y \to x}(x, y). \quad (4.4)$$

The rate $\omega(y)$ will be proportional to the effective cutting frequency λ per unit time and length. It will also be proportional to the length, respectively, of elements of class y:

$$\omega(y) = \lambda y. \tag{4.5}$$

The density $P_{y \to x}$ can be evaluated by imagining an element of class y which is subdivided by the cutting process in such a way that an element of class x is generated. Since the number of grid cells generated by this process is proportional to the number of grid cells in the element of class x, and since the number of grid cells within the element of class x is uniformly distributed, the probability density $P_{y \to x}(x, y)$ is proportional to x:

$$P_{y \to x} = A x. \tag{4.6}$$

Here A is the normalization factor to be determined from

$$\int_0^y A x \, \mathrm{d}x = 1, \tag{4.7}$$

since x may vary between $x = 0$ and $x = y$. From integration we readily obtain

$$P_{y \to x} = 2 \frac{x}{y^2}. \tag{4.8}$$

The time rate of change due to the (gc) process is then

$$\frac{\partial}{\partial t} [n_x P_x]_{\mathrm{gc}} = 2 \lambda \int_x^\infty \frac{x}{y} n_y P_y(y, t) \, \mathrm{d}y. \tag{4.9}$$

Next we consider the removal (rc) of grid cells by cutting an element of class x to smaller elements of other classes. The time rate of change of $n_x P_x$ due to this process is

$$\frac{\partial}{\partial t} [n_x P_x]_{\mathrm{rc}} = -n_x P_x \int_0^x W_{\mathrm{rc}}(y|x) \, \mathrm{d}y, \tag{4.10}$$

where

$$W_{\mathrm{rc}}(y|x) = \omega(x) P_{x \to y}. \tag{4.11}$$

The rate $\omega(x)$ of this transition will now be proportional to x. Instead of (4.5) we therefore have $\omega(x) = \lambda x$. The probability density of transitions $P_{x \to y}$ will be independent of y and uniform in $0 \leqslant y \leqslant x$ with the normalization condition

$$\int_0^x P_{x \to y} \, \mathrm{d}y = 1. \tag{4.12}$$

Therefore the time rate of change of the (rc) process becomes

$$\frac{\partial}{\partial t} [n_x P_x]_{\mathrm{rc}} = -\lambda x n_x P_x. \tag{4.13}$$

Let us now consider the generation of elements by the reconnection process (gr). It is due to the generation of larger elements of class x from a smaller element of class y when extremal points are removed by the disappearance of very small elements. In figure 8 the smallest element would disappear by diffusion, thereby reconnecting its nearest neighbours. The time rate of change of $n_x P_x$ due to this process is

$$\frac{\partial}{\partial t} [n_x P_x]_{\mathrm{gr}} = \int_0^x W_{\mathrm{gr}}(x|y) n_y P(y, t) \, \mathrm{d}y. \tag{4.14}$$

Since elements of class y cannot become larger than those of the fixed class x the integration is performed between 0 and x.

The two extremal points of the very small elements will merge with each other and disappear when the reconnection occurs. Attached to the two extremal points are two adjacent elements. We will denote the rate of reconnection at each extremal point by μ. Therefore the transition probability density per unit time of this process is

$$W_{gr}(x|y) = 2\mu P_{y\to x}(x, y). \tag{4.15}$$

The probability density $P_{y\to x}$ is equal to

$$P_{y\to x} = P_z(x - y, t), \tag{4.16}$$

where $z = x - y$ is the class of elements that combine with an element of class y to form an element of class x. We therefore obtain for the time rate of change due to the (gr) process

$$\frac{\partial}{\partial t}[n_x P_x]_{gr} = 2\mu \int_0^x P_z\,(x - y, t)n_y P_y(y, t)\,\mathrm{d}y. \tag{4.17}$$

It may be noted that, apart from the factor n_y, the integral on the right-hand side is the convolution of the statistically independent densities $P_y(y)$ and $P_z(z)$ resulting in the density $P_x(x)$ that one obtains for the addition of random variables y and z according to $y + z = x$.

Finally, the time rate of change of $n_x P_x$ by the removal of one of the two smaller elements of class x by the reconnection process (rr) is

$$\frac{\partial}{\partial t}[n_x P_x]_{rr} = -2\mu n_x P_x \tag{4.18}$$

following arguments similar to those that led to (4.13)

Since the probability densities of the three classes of elements x, y and z are equal to each other we will introduce the notation $P(x, t)$ without index:

$$P_x(x, t) = P_y(y, t) = P_z(z, t) \equiv P(x, t). \tag{4.19}$$

Furthermore, the number of grid cells n_x and n_y within the elements is proportional to x and y, respectively, for a uniform mesh. Since the proportionality factors cancel when n_x and n_y are inserted into the terms of (4.2) one obtains, after division by x, for the time rate of change of the probability density $P(x, t)$

$$\frac{\partial P(x, t)}{\partial t} = 2\lambda \int_0^\infty P(x + z, t)\,\mathrm{d}z - \lambda x\,P(x, t)$$
$$+ 2\mu \int_0^x \frac{y}{x}P(x - y, t)P(y, t)\,\mathrm{d}y - 2\mu P(x, t). \tag{4.20}$$

Here we have replaced y by $y = x + z$ in (4.9) to obtain the first integral in a more convenient form. The steady-state solution of this equation should yield the exponential distribution describing the probability density of the distance between two Poisson points along a line (Papoulis 1991, p. 355)

$$P(x) = \rho \exp(-\rho x), \tag{4.21}$$

where $\rho = 1/\langle x \rangle$ is the mean number of elements per unit length with $\langle x \rangle$ being the average length of elements. For the steady-state Poisson process the rates of additions and removals of Poisson points per unit length are equal:

$$\lambda = \mu \rho. \tag{4.22}$$

It is easily verified that, with this, (4.21) satisfies the steady-state form of (4.20). Note that in this case the (gc) term balances the (rr) term and the (gr) term balances the (rc) term thereby creating a cross-link between the cutting and the reconnection processes.

We now consider the drift process that follows from the annihilation of a minimum and a maximum point by diffusion. The velocities of extremal points relative to each other is due to the following two contributions already described by Gibson (1968).

(a) The displacement speed $v_D(x)$ due to the diffusion of scalar isolines. This speed scales, for small values of x, with the diffusivity D as

$$v_D(x) = \frac{\mathrm{d}x}{\mathrm{d}t} = -\frac{D}{x} \quad \text{for} \quad x \to 0, \tag{4.23}$$

which is the velocity at which the very small elements drift to the origin. This indicates that $v_D(x)$ is negative for small elements but must change sign and become positive for larger elements. In order to account for this we introduce the ansatz

$$v_D(x) = -\frac{D}{x} \left[1 - c \left(1 - \exp(-2\rho x) \right) \right]. \tag{4.24}$$

The exponential decay rate of 2ρ was chosen to agree with velocity data from one-dimensional simulations. Note that v_D is singular at the origin. This singularity requires $P(x)$ to be proportional to x at the origin, a property that we will use below.

(b) The relative velocity $v(x)$ of the two extremal points. This velocity is a stochastic variable whose mean value should depend on the element class x. We introduce the mean compressive strain rate $\bar{a}(x)$ by

$$v(x) = -\bar{a}(x)\, x. \tag{4.25}$$

An overall compression of the axis of linearly arranged elements will increase the number of elements in each class at a rate proportional to the compression rate, cf. Peters & Trouillet (2002),

$$\frac{\partial P(x,t)}{\partial t} = \bar{a}(x)\, P(x,t). \tag{4.26}$$

Therefore we also have to add a source term $\bar{a}(x)\, P(x,t)$ on the right-hand side of (4.20).

Since the ensemble of elements must conserve the total length L we have the additional condition

$$\frac{\mathrm{d}L}{\mathrm{d}t} = \int_0^\infty (v_D(x) + v(x))\, P(x)\, \mathrm{d}x = 0. \tag{4.27}$$

Since the reconnection process is caused by the disappearance of the very small elements at the origin $x = 0$, the reconnection rate μ must be associated with this disappearance. During a small time span Δt elements of the classes $0 < x < \Delta x$ drift to the origin and disappear there such that, by integration of (4.23), Δx is related to Δt:

$$(\Delta x)^2 = 2D\Delta t. \tag{4.28}$$

The number of small elements disappearing is, in the limit $\Delta x \to 0$,

$$\int_0^{\Delta x} P(x)\, \mathrm{d}x = \int_0^{\Delta x} x \left.\frac{\partial P}{\partial x}\right|_{x=0} \mathrm{d}x = \frac{(\Delta x)^2}{2} \left.\frac{\partial P}{\partial x}\right|_{x=0}, \tag{4.29}$$

since $P(0) = 0$. This number is proportional to the reconnection rate μ times the time span Δt, namely $\mu \Delta t$. With (4.28) and (4.29) this leads to

$$\mu = D \frac{\partial P}{\partial x}\bigg|_{x=0}. \qquad (4.30)$$

Using this and adding the two drift terms and the source term to (4.20), after normalization of $v_D(x)$, $\bar{a}$, P and x, y and z by the mean value $\langle x \rangle = 1/\rho$ and D according to

$$\tilde{x} = \rho x, \; \tilde{y} = \rho y, \; \tilde{z} = \rho z, \; \tilde{v}_D = v_D/(\rho D), \; \tilde{a} = \bar{a}/(\rho^2 D), \; \tilde{P}(\tilde{x}, t) = P(x, t)/\rho, \quad (4.31)$$

one obtains the final equation

$$\frac{\partial \tilde{P}(\tilde{x}, t)}{\partial t} + \frac{\partial [\tilde{v}_D(\tilde{x}) P(\tilde{x}, t)]}{\partial \tilde{x}} - \frac{\partial [\tilde{a}\tilde{x} P(\tilde{x}, t)]}{\partial \tilde{x}} = \Lambda \left[2 \int_0^\infty \tilde{P}(\tilde{x} + \tilde{z}, t) \, \mathrm{d}\tilde{z} - \tilde{x} \tilde{P}(\tilde{x}, t) \right]$$
$$+ 2 \frac{\partial \tilde{P}}{\partial \tilde{x}}\bigg|_{\tilde{x} \to 0} \left[\int_0^{\tilde{x}} \frac{\tilde{y}}{\tilde{x}} \tilde{P}(\tilde{x} - \tilde{y}, t) \tilde{P}(\tilde{y}, t) \, \mathrm{d}\tilde{y} - \tilde{P}(\tilde{x}, t) \right] + \tilde{a}(\tilde{x}) P(\tilde{x}, t). \quad (4.32)$$

Here Λ is a Péclet number defined by

$$\Lambda = \frac{\lambda}{\rho^3 D}. \qquad (4.33)$$

In the steady-state case it determines the mean value $\langle x \rangle = 1/\rho$. Equation (4.32) must satisfy the normalization condition

$$\int_0^\infty \tilde{P}(\tilde{x}, t) \, \mathrm{d}x = 1. \qquad (4.34)$$

In principle, this evolution equation can describe the build-up of the length-scale distribution starting from an initial condition (a delta function at a large length, for instance) or the disappearance of elements once the cutting process stops. The latter will be the case in decaying isotropic turbulence where the solution for the final homogeneous mixture will be a delta function at the origin. Here, for the case of continuous steady forcing by turbulence with a mean scalar gradient we are looking for a steady-state solution for $t \to \infty$ where the solution must also satisfy the condition that the mean value is constant and therefore that of the normalized variable $\tilde{x}$ should be unity:

$$\int_0^\infty \tilde{x} \tilde{P}(\tilde{x}) \, \mathrm{d}x = 1. \qquad (4.35)$$

Since the mean compressive strain rate for dissipation elements cannot be derived from first principles we consider the case $\tilde{a}(\tilde{x}) = 0$. Then (4.27) applies to $v_D(x)$ only and determines the constant c. The steady-state solution of (4.32) has been calculated numerically by a finite difference method. An unsteady solution method was applied for a chosen value of Λ, which converged to a steady state by applying the normalization condition at each time step. The value of Λ was then varied until (4.35) was satisfied. We obtain $\Lambda = 5.5$ and $c = 1.92$ as part of the solution.

The comparison of this solution with the marginal p.d.f. (3.2) for case 2 as an example is shown in figure 9. Here the length scale was normalized with the mean value l_m. These were obtained from each p.d.f. generated by DNS and are listed in table 1. Both p.d.f.s show a steep rise at the origin and an exponential decay for large values of l/l_m. The inset log-linear plot shows that the slope of the exponential is
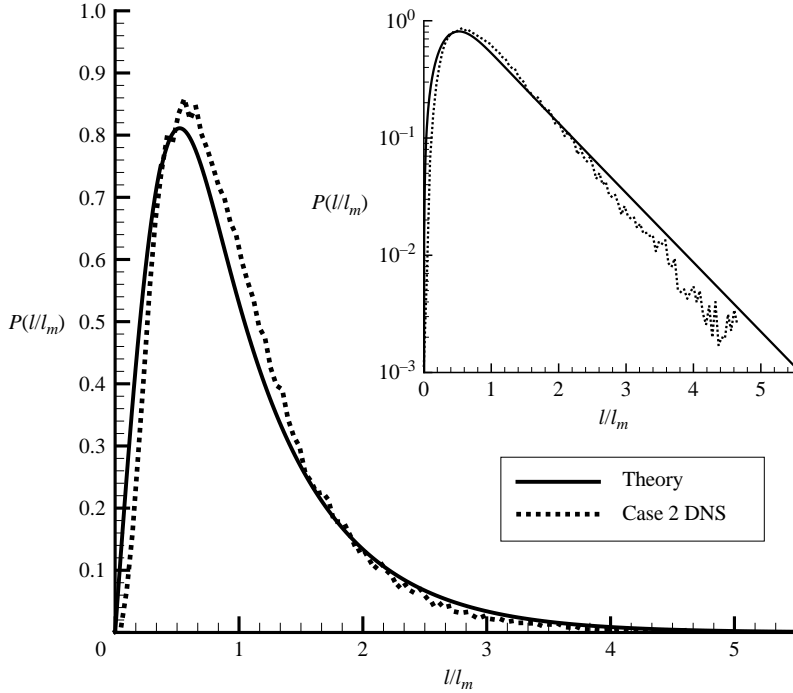
FIGURE 9. The marginal p.d.f. from the DNS for case 2 compared to theoretical predictions for zero and unity normalized compression rates.

somewhat steeper in the three-dimensional DNS data than in the one-dimensional theory. Nevertheless, the agreement between the theoretically derived p.d.f. solution and those from the DNS is satisfactory.

The comparison of the length scales listed in table 1 shows that l_m is much larger than the Kolmogorov scale but of the order of the Taylor scale. In order to demonstrate this (see the companion paper, Peters & Wang 2005) a stochastic one-dimensional simulation from which we conclude that the cutting frequency per unit length λ multiplied by l_m should be of the order of the inverse of the integral time scale $\tau = k/\varepsilon$. Then (4.33) with $\rho = l_m^{-1}$ substituted results in

$$l_m \propto (D\tau)^{1/2} \propto (\nu k/\varepsilon)^{1/2} \propto \lambda, \qquad (4.36)$$

showing that the mean length should indeed be of the order of the Taylor scale.

5. Conclusions

Having chosen a method of numerically identifying random geometrical elements in scalar turbulence we were able to answer the first of Corrsin's questions quoted in the introduction: that a naturally identifiable geometry is our dissipation elements. We have in this paper tried to answer the second question on the role they play. The third question has also be addressed by inventing a stochastic 'game' of cutting and reconnecting such random elements.

The gradient trajectory method that we have introduced here is able to identify finite-size regions in a turbulent scalar field without arbitrariness. It is interesting that the resulting dissipation elements, though they may appear convoluted by comparison

to vortex filaments, still obey on the average some basic rules: (i) Their linear length-scale distribution function agrees with the theoretically derived distribution function; (ii) the conditional mean of the scalar difference follows the Kolmogorov scaling over a larger range than the classical structure function.

REFERENCES

ASHURST, W. T., KERSTEIN, A. R., KERR, R. M. & GIBSON, C. H. 1987 Alignment of vorticity and scalar gradient with strain rate in simulated Navier-Stokes turbulence. *Phys. Fluids* **30**, 2343–2353.

CORRSIN, S. 1971 Random geometric problems suggested by turbulence. In *Statistical Models and Turbulence*. Lecture Notes in Physics, vol. 12 (ed. M. Rosenblatt & C. Van Atta), pp. 300–316. Springer.

D'ACUNTO, D. & KURDYKA, K. 2004 Bounds for gradient trajectories of polynomials and definable functions with applications. *J. Diffl Geom.* (submitted).

FRISCH, U. 1995 *Turbulence: The Legacy of A.N. Kolmogorov*. Cambridge University Press.

GIBSON, C. H. 1968 Fine structure of scalar fields mixed by turbulence I. Zero gradient points and minimal gradient surfaces. *Phys. Fluids* **11**, 2305–2315.

JIMENEZ, J. & WRAY, A. 1998 On the characteristics of vortex filaments in isotropic turbulence. *J. Fluid Mech.* **373**, 255–285.

MENEVEAU, C. & SREENIVASAN, K. 1991 The multifractal nature of turbulent energy dissipation. *J. Fluid Mech.* **224**, 429–484.

MIYAUCHI, T. & TANAHASHI, M. 2001 Coherent fine scale structure in turbulence. In *IUTAM Symp. on Geometry and Statistics of Turbulence* (ed. T. Kambe *et al.*), pp. 67–75. Kluwer.

MOFFATT, H. K. 2001 The topology of scalar fields in 2d and 3d turbulence. In *IUTAM Symp. on Geometry and Statistics of Turbulence* (ed. T. Kambe *et al.*), pp. 13–22. Kluwer.

PANTANO, C., SARKAR, S. & WILLIAMS, F. 2003 Mixing of a conserved scalar in a turbulent reacting shear layer. *J. Fluid Mech.* **481**, 291–328.

PAPOULIS, A. 1991 *Probability, Random Variables and Stochastic Processes*, 3rd edn. McGraw-Hill.

PETERS, N. 2000 *Turbulent Combustion*. Cambridge University Press.

PETERS, N. & TROUILLET, P. 2002 On the role of quasi-one-dimensional dissipation layers in turbulent scalar mixing. *Annual Research Briefs, Center for Turbulence Research, Stanford University*, pp. 27–40.

PETERS, N. & WANG, L. 2005 Dissipation element analysis of scalar fields in turbulence. *C. R. Mechanique* (submitted).

POPE, S. 2000 *Turbulent Flows*. Cambridge University Press.

ROGERS, M. & MOSER, R. 1994 Direct numerical simulation of a self-similar turbulent mixing layer. *Phys. Fluids* **6**, 903–923.

SARKAR, S. 1995 The stabilizing effect of compressibility in turbulent shear flow. *J. Fluid Mech.* **282**, 163–186.

TOWNSEND, A. 1951 On the fine structure of turbulence. *Proc. R. Soc. Lond.* A **208**, 534–542.

TSINOBER, A. 2001 *An Informal Introduction to Turbulence*. Kluwer.

VAN KAMPEN, N. G. 1992 *Stochastic Processes in Physics and Chemistry*. Elsevier.

WRAY, A. & HUNT, J. 1990 Algorithms for classification of turbulent structures. In *Topological Fluid Mechanics* (ed. H. Moffat & A. Tsinober), pp. 95–104. Cambridge University Press.